Supporting Information

Room-temperature ferroelectric and ferroelastic orders coexisting in a new tetrafluoroborate-based perovskite

Xiao-Xian Chen, [a] Xiao-Yue Zhang, [b] De-Xuan Liu, [a] Rui-Kang Huang, [a] Sha-Sha Wang, [a] Li-Qun Xiong, [b] Wei-Xiong Zhang,*[a] and Xiao-Ming Chen [a]

[a]MOE Key Laboratory of Bioinorganic and Synthetic Chemistry, School of Chemistry, Sun Yat-Sen University, Guangzhou 510275, China

[b]State Key Laboratory of Optoelectronic Materials and Technologies, School of Physics, Sun Yat-Sen University, Guangzhou 510275, China

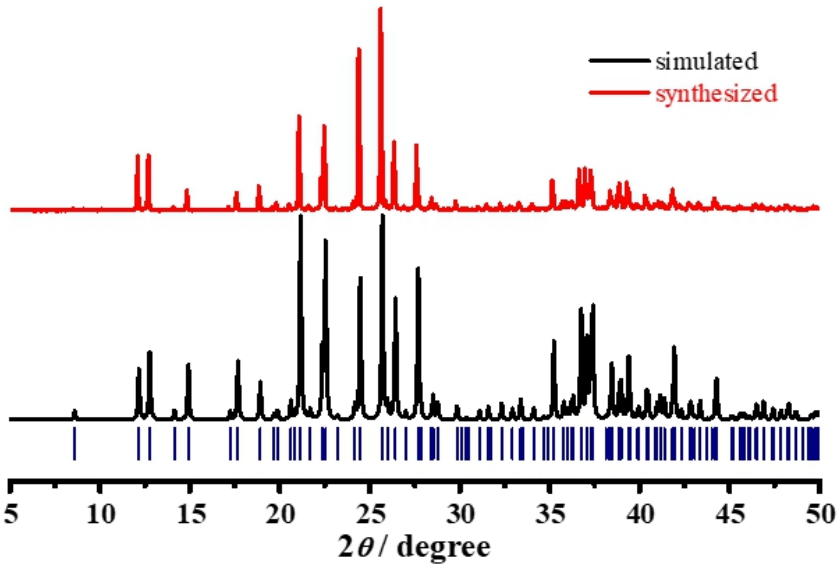

Fig. S1 The experimental PXRD pattern (red) on the as-synthesized powder sample and the simulated PXRD pattern (black) based on the single-crystal structure of room-temperature phase.

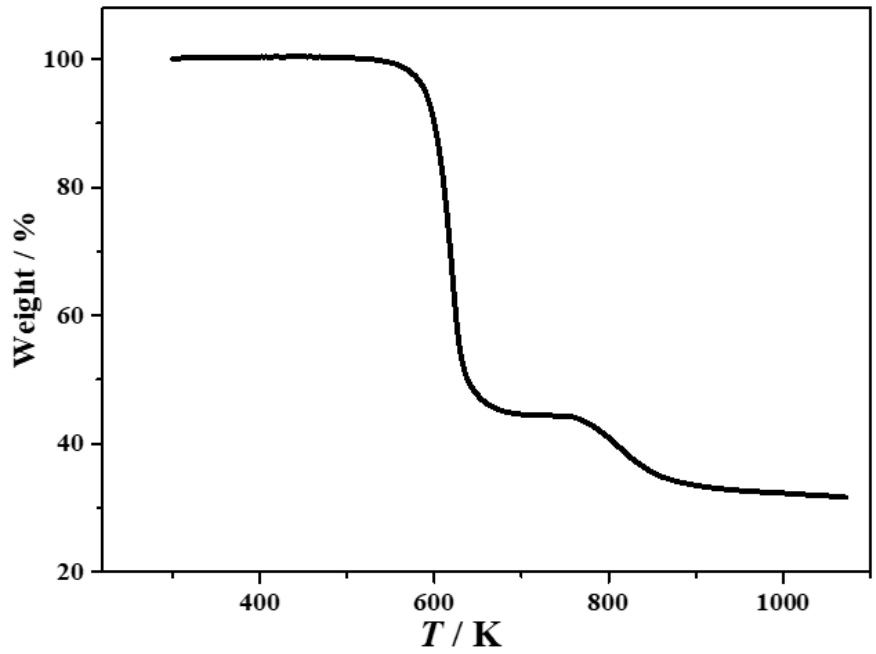

Fig. S2 TG profile of **1**.

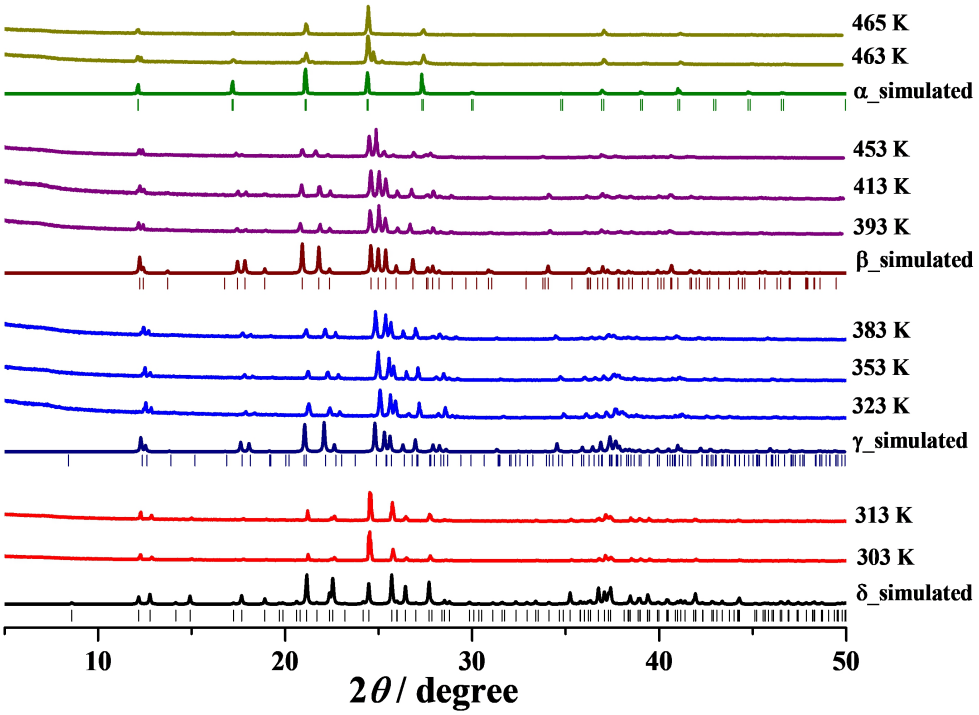

Fig. S3 The variable-temperature experimental PXRD patterns of **1** and the simulated patterns based on single-crystal structures for the four phases.

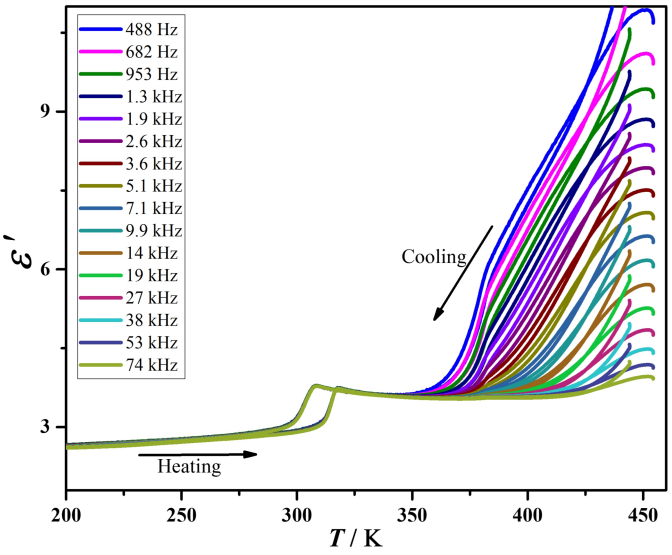

Fig. S4 The real part of the dielectric permittivity during a heating-cooling cycle in the temperature range of 200-450 K on the powder-pressed sample of **1**, by applying ac field with variable frequencies from 500 Hz to 74 kHz.

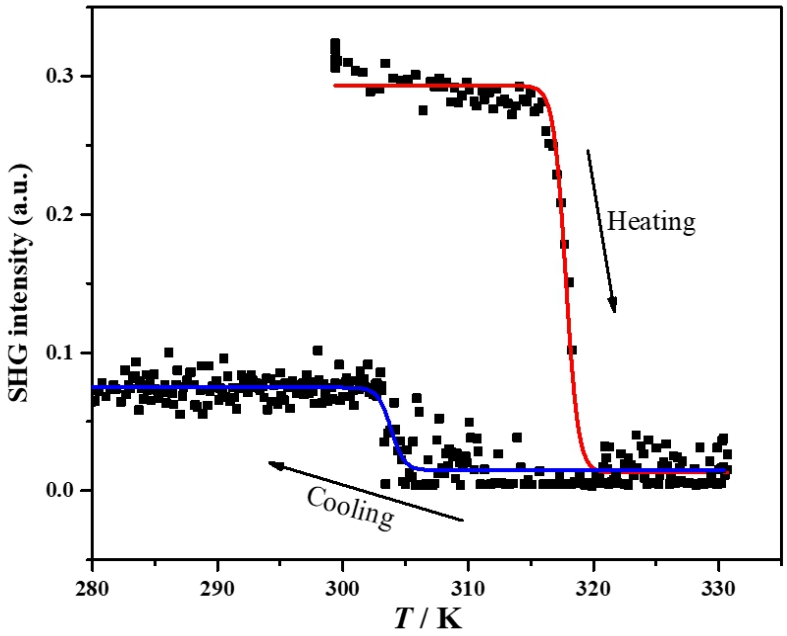

Fig. S5 Temperature-dependence of SHG signal during a heating and cooling cycle between 290 K and 330 K for **1**. The SHG intensity of α phase during cooling run was not recovered, probably owing to a fact that the crystal sample size was decreased after cooling across the ferroelectric phase transition.

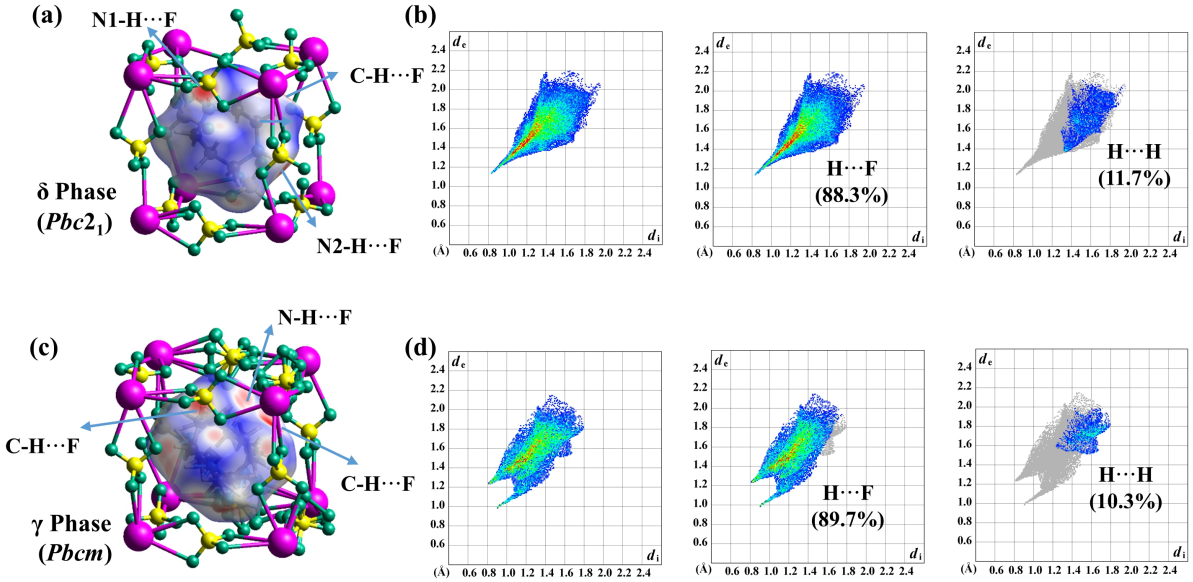

Fig. S6 Hirshfeld surfaces mapped with d_{norm} over the range of −0.50 (red) to 0.90 (blue) for the guest cation in δ phase (a) and γ phase (c). Fingerprint plots for all contacts, H···F contacts and H···H contacts of guest cations in δ phase (b) and γ phase (d).

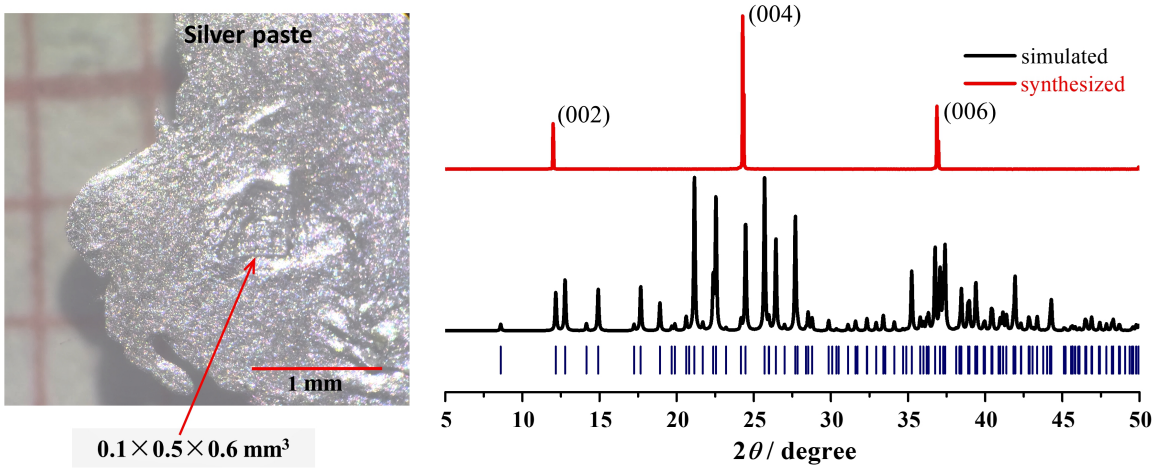

Fig. S7 The size (left) and X-ray diffraction patterns (right) measured on the largest plane of single crystal for PFM tests. Only the (002) reflection clusters were observed, indicating the normal of the largest plane of the single crystal is the *c*-axis.

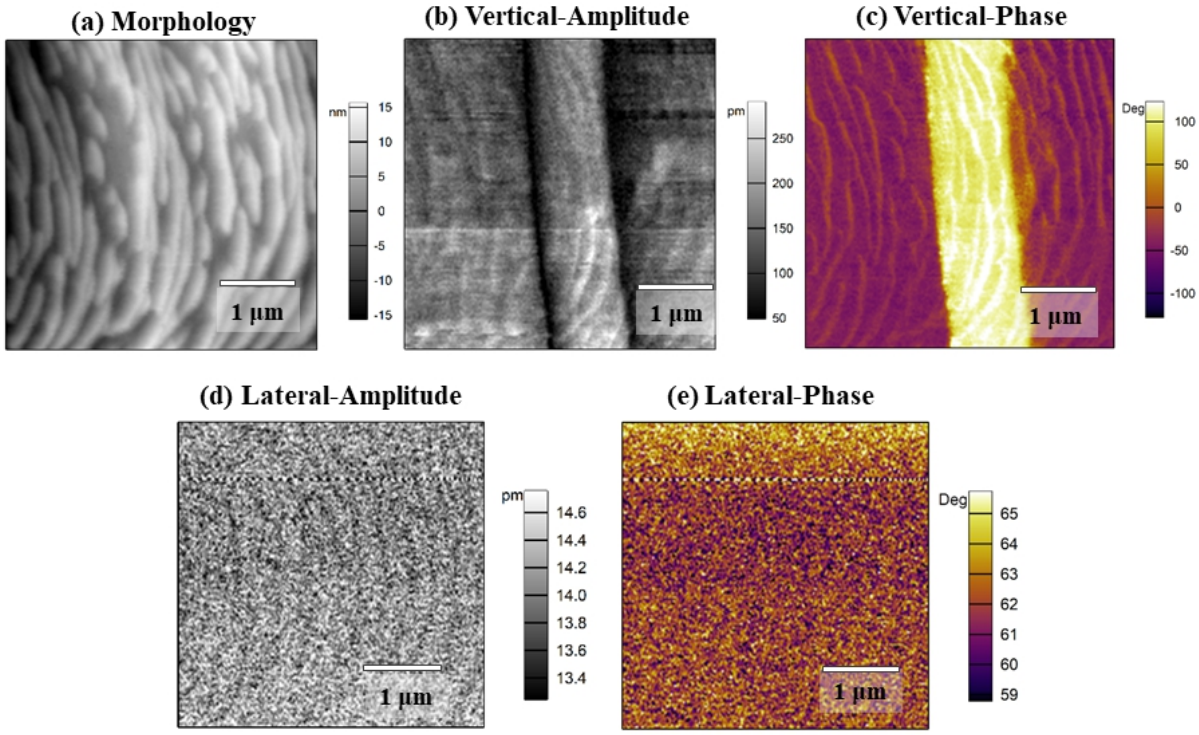

Fig. S8 Morphology image (a), vertical (b, c) and lateral (d, e) PFM images of the sample surface for **1**.

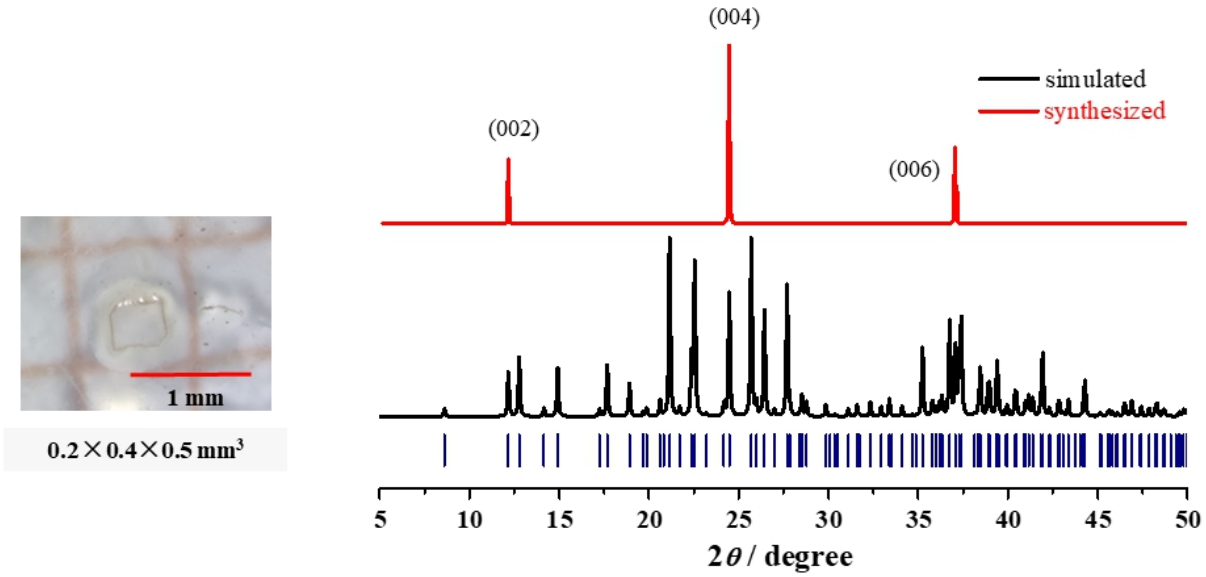

Fig. S9 The size (left) and X-ray diffraction patterns (right) measured on the largest plane of single crystal for observation of ferroelastic domains.

Deformation of framework.

The deformations of framework occur in β, γ, and δ phases. The framework deformation in perovskite structure include three parts: (1) shifts of columns of connected BX_6 octahedra, (2) rotation of octahedra, and (3) B-site displacements inside the octahedra, called as shifts, tilts, and displacements, respectively. For description of shifts and tilts, an extended Glazer's notations was developed recently. [S1-S4] As manifested in these extended notations, both shifts and tilts descriptors take the form of a 3×3 matrix, where the terms are associated with distortion periodicity and can be determined by viewing along the relevant pseudo-cubic axis or viewing in the corresponding plane after taking slices of the structure (Fig. S10). The full tilt matrix is constructed by generalized Glazer terms $g_{xy} = \varepsilon_x \exp[2\pi i k_{xy}]$, where x and y belong to one of three pseudo-cubic axes, a_p, b_p, c_p, indicating the correlation of rotations around x-axis propagating in y-axis. In the terms, ε_x with a value of 0 or 1 means the tilt is inactive or active, while k, the wave vector of the propagation, means the periodicity of the tilt propagating in the relevant direction, with the most common values in an active tilt, $k = 0$ ($g = 1$, labeled as "+" by convention) indicating in-phase propagation or $k = 1/2$ ($g = -1$, labeled as "−" by convention) indicating out-of-phase propagation. It should be noted that the tilt matrix can be characterized by a conventional Glazer notation when all the off-diagonal terms ($x \neq y$) are "−". Similarly, the full shift matrix is constructed by terms $\mu_{xy} = u_x \exp[2\pi i k_{xy}]$, indicating the correlation of columnar shifts parallel to x-axis propagating in y-axis. Specially, the values of μ_{xy} are either 0 or 1 when $x = y$, indicating an inactive or active shift along the relevant axis, respectively.

Thus, the value of terms in the matrix and its meaning are as follows:

0 $\varepsilon_x = 0$ (or $u_x = 0$) inactive tilts (or shifts)

\+ $\varepsilon_x = 1$ (or $u_x = 1$), $k_{xy} = 0$ active in-phase tilts (or shifts)

− $\varepsilon_x = 1$ (or $u_x = 1$), $k_{xy} = 1/2$ active out-of-phase tilts (or shifts)

For convenience of description and comparison, the BF_4^- bridges are simplified as a mono-atomic X-site node using its central boron atom to form KB_6 octahedra and most matrices are given by a Glazer's or extended Glazer's notation as shown in Fig. S10. Specially, an unconventional tilt exists in the β phase even if BF_4^- bridges are topologically regarded as mono-atomic X-site nodes. Compared with conventional tilt in the inorganic perovskites, such unconventional tilt in molecular perovskite occurs because the coexistent shifts distortion allows the in-phase propagations ("+") of tilts in a_p- and in b_p-axes.

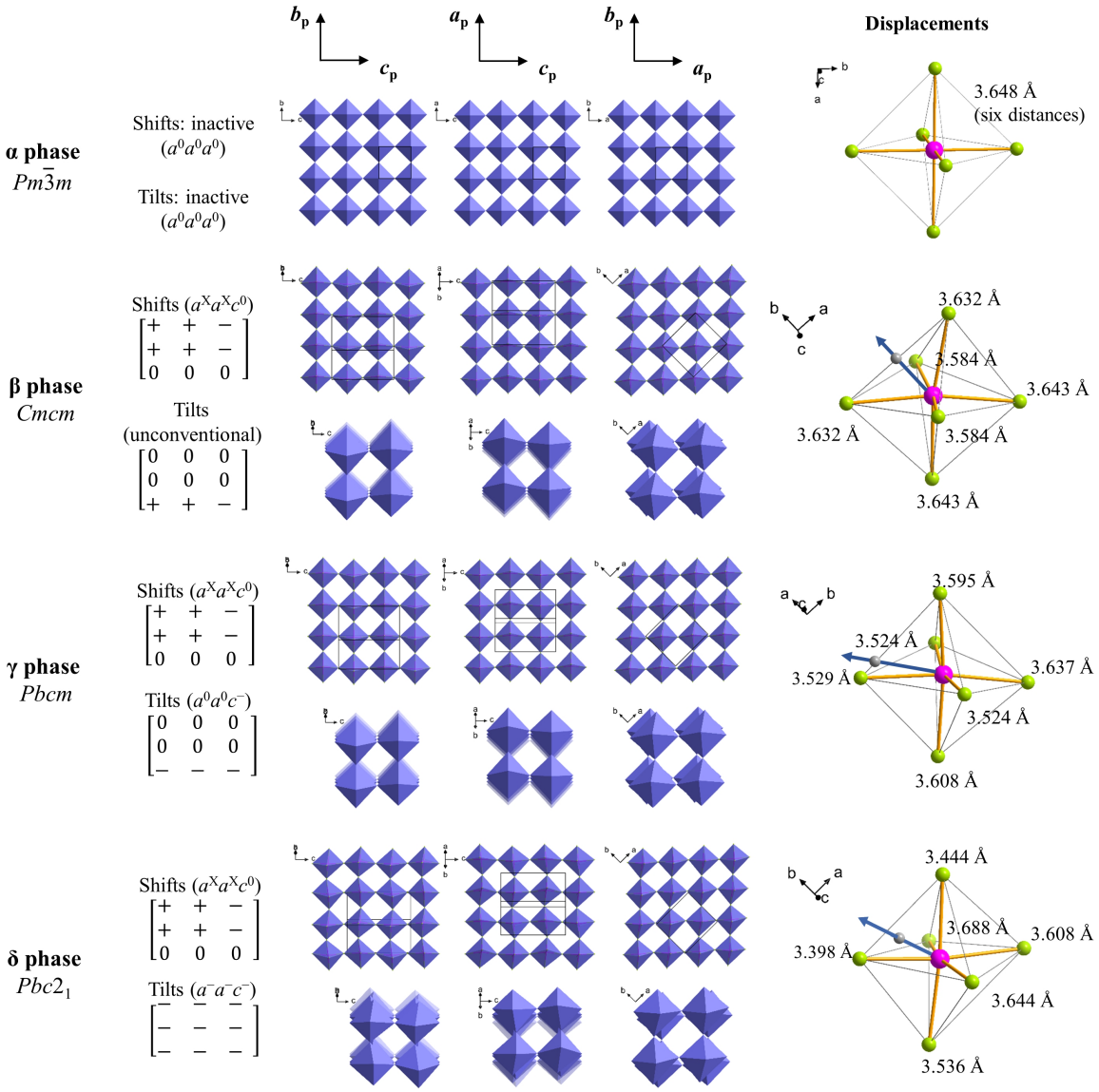

Fig. S10 Tilts, shifts, and displacements in β, γ and δ phases. For comparison, the regular octahedra of α phase without deformation are shown as well. For each phase, the types of tilts and shifts (left) can be determined by single 4×4 octahedral layers and 2×2×4 stacks (middle) viewed normal to the three pseudo-cubic perovskite axes (labeled as a_p, b_p, or c_p). Specifically, the 4×4 layers show the in-plane tilt/shift and the 2×2×4 stacks show the in-axis tilt. The direction of displacements is indicated by blue arrow and six distances between B-site K^+ ion and X-site bridges are noted for assistance to the determination of the direction (right). For clarity, F atoms are omitted and BF_4^- bridges are simplified into aqua nodes.

The calculation of the spontaneous strain

For the present *m*3*m*F*mmm*(*ss*) species, six orientation states (S_1, S_2, S_3, S_4, S_5, S_6) are possible for the orthorhombic phase, and the spontaneous strain tensor ε_s for the six states is given as[S5-S6]

$$\varepsilon_s(S_1) = \begin{bmatrix} -2e & 0 & 0 \\ 0 & e & d \\ 0 & d & e \end{bmatrix} \qquad \varepsilon_s(S_2) = \begin{bmatrix} -2e & 0 & 0 \\ 0 & e & d \\ 0 & d & e \end{bmatrix} \qquad \varepsilon_s(S_3) = \begin{bmatrix} e & 0 & d \\ 0 & -2e & 0 \\ d & 0 & e \end{bmatrix}$$

$$\varepsilon_s(S_4) = \begin{bmatrix} e & 0 & -d \\ 0 & -2e & 0 \\ -d & 0 & e \end{bmatrix} \quad \varepsilon_s(S_5) = \begin{bmatrix} e & d & 0 \\ d & e & 0 \\ 0 & 0 & -2e \end{bmatrix} \quad \varepsilon_s(S_6) = \begin{bmatrix} e & -d & 0 \\ -d & e & 0 \\ 0 & 0 & -2e \end{bmatrix}$$

The proportional relationships between the magnitude of the lattice parameters in the ferroelastic phase (a, b, c) and the prototype phase (a_p, b_p, c_p) are[S7]

$$a = \sqrt{2}a_p$$

$$b = \sqrt{2}b_p$$

$$c = 2c_p$$

The spontaneous strain for both $m3mFmmm(ss)$ and $m3mFmmm(pp)$ species is given as[S7]

$$\varepsilon_s = \sqrt{(2a_p^2 + 2b_p^2 + 2c_p^2 - 2a_pb_p - 2b_pc_p - 2a_pc_p)/(3a_0^2)}$$

where a_0 is the lattice parameter of the cubic phase (α).

As the proportional relationships between the magnitude of the lattice parameters in the ferroelastic phase and the prototype phase should be considered, the spontaneous strain for the present α→β ferroelastic transition is

$$\varepsilon_s = \sqrt{(2a^2 + 2b^2 + c^2 - 2ab - \sqrt{2}ac - \sqrt{2}bc)/(6a_0^2)} = 0.0459$$

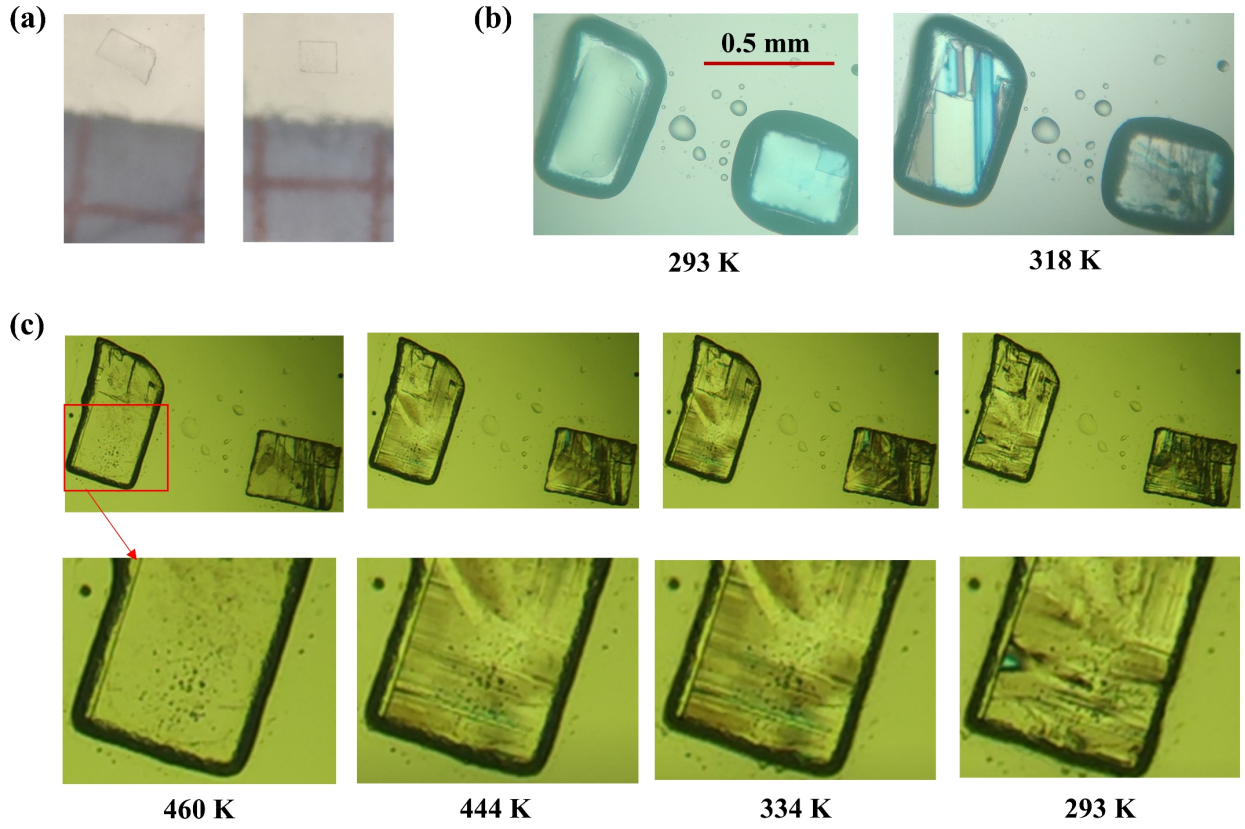

Fig. S11 (a) Photos of the two tested single crystals on paper under an optical microscope at room temperature. (b) Photos taken using a polarizing microscope at room temperature (293 K) and after heating through the ferroelectric phase transition to 318 K. (c) Photos taken using a polarizing microscope in a cooling run from a paraelastic phase (at 460 K) to ferroelastic phase (at 444, 334, and 293 K, respectively). The pictures below show a zoom-in area of single crystal to show the detail of the domains evolution during the ferroelastic transitions.

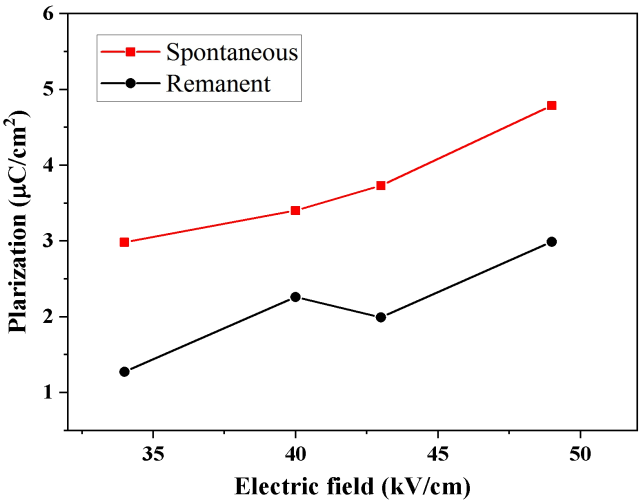

Fig. S12 Electric field dependence of spontaneousand remanent polarization of **1**.

Table S1. Hydrogen bonds in δ phase and γ phase.

	D–H	A	*d*(D–H) /Å	*d*(H–A) /Å	*d*(D–A) /Å	D–H–A /°
δ phase	N1–H1A	F23[a]	0.89	2.29	3.048(5)	142.4
	N1–H1A	F34[b]	0.89	2.19	2.882(4)	134.7
	N1–H1B	F33	0.89	2.08	2.945(5)	164.4
	N2–H2A	F12[c]	0.89	2.38	3.190(5)	151.7
	N2–H2A	F21[c]	0.89	2.43	3.011(5)	123.7
	N2–H2B	F12[d]	0.89	2.20	2.953(4)	142.8
	N2–H2B	F24[d]	0.89	2.48	3.149(5)	132.3
	C2–H2D	F11[e]	0.97	2.41	3.251(5)	145.0
	C2–H2D	F21[c]	0.97	2.65	3.247(6)	120.4
	C5–H5B	F32[a]	0.97	2.35	3.128(6)	137.0
γ phase	N2–H2A	F32	0.89	2.43	3.09(3)	131.4
	N2–H2B	F34	0.89	2.55	3.30(3)	141.7
	C2–H3B	F22	0.97	2.69	3.301(11)	121.1
	C4–H4A	F22	0.97	2.59	3.311(15)	131.0

Symmetric codes: A) +X, 1/2−Y, 1/2+Z; B) 1−X, −1/2+Y, +Z; D) +X, 3/2−Y, 1/2+Z.

References

(S1) A. M. Glazer, *Acta Cryst.*, 1972, **B28**, 3384-3392.

(S2) A. L. Goodwin, *Phys. Rev. B*, 2006, **74**, 134302.

(S3) H. L. Bostrom, J. A. Hill, A. L. Goodwin, *Phys. Chem. Chem. Phys.*, 2016, **18**, 31881-31894.

(S4) Y. Wu, T. Binford, J. A. Hill, S. Shaker, J. Wang, A. K. Cheetham, *Chem. Commun.* 2018, **54**, 3751-3754.

(S5) K. Aizu, *J. Phys. Soc. Jpn.*, 1970, **28**, 706-716.

(S6) J. Sapriel, *Phys. Rev. B*, 1975, **12**, 5128-5140.

(S7) Y. Zhao, D. J. Weidner, J. B. Parise, D. E. Cox, *Phys. Earth Planet. In.*, 1993, **76**, 17-34.